



SMHIGridClim, 2.5 km resolution gridded climatology of Fennoscandia

Sandra Andersson, Maria Norman, Tomas Landelius, Patrick Samuelsson, Semjon Schimanke, Maida Zahid, Lars Barring

5 Swedish Meteorological and Hydrological Institute (SMHI), Norrköping, 601 76, Sweden

Correspondence to: Sandra Andersson (sandra.andersson2@smhi.se)

Abstract.

SMHIGridClim, the Swedish Meteorological and Hydrological Institute Gridded Climatology, covers Fennoscandia at 2.5 km horizontal resolution for the period 1961–2018. It includes two-meter temperature and two-meter relative humidity at 1-, 3-, or 6-hour temporal resolution (which varies over the covered period), as well as daily minimum and maximum temperatures, daily precipitation, and daily snow depth. The gridding is performed using optimal interpolation with the open-source software gridpp from the Norwegian Meteorological Institute. Observations used in the analysis are provided by the Swedish, Finnish, and Norwegian meteorological institutes, as well as the European Centre for Medium-Range Weather Forecasts (ECMWF). Quality control of the observations is conducted using the open-source software TITAN, also developed at the Norwegian Meteorological Institute. The first guess for the optimal interpolation is obtained from the UERRA-HARMONIE reanalysis at 11 km horizontal resolution, which is statistically downscaled to fit a subset of the operational MEPS numerical prediction system at 2.5 km horizontal resolution, with daily and yearly variations in the downscaling parameters. The quality of the analysis varies over time and depends on both the accuracy of forecasts and the quality and density of available observations. In terms of annual mean root mean square error (RMSE), the quality of SMHIGridClim is comparable to similar gridded datasets covering the Nordic countries. SMHIGridClim is available at <https://doi.org/10.7910/DVN/ZFZL6K> (Andersson et al., 2025).

1 Introduction

Gridded climate datasets with high resolution and long-term coverage have become vital for climatological and environmental research (Brohan et al., 2006; Alto et al.; 2016; IPCC 2021). These datasets enable researchers to assess climate change and its impacts, providing valuable insights for formulating sustainable approaches to climate



challenges (Overpeck et al., 2011). Compared to point data, gridded datasets offer several advantages as they are generally user-friendly, offer mostly uniform spatial coverage, ensure consistent temporal coverage and seldom have missing data (Essou et al., 2016). Even so, they have their drawbacks (e.g., real-time availability and potential
30 inaccuracies in regions with sparse observation networks) that make them inadequate for many applications in regions with complex topography (Zandler et al., 2019; Mankin et al., 2024). Moreover, gridded datasets often lack consistency between variables. The exception is reanalysis datasets which are based on dynamical models.

Northern regions, particularly the Arctic areas are at the forefront of climate change discussions due to their rapid warming (IPCC, 2013; Fountain et al., 2012). The climate change signal is also quite noticeable across the
35 Fennoscandia (Finland, Sweden and Norway), with altered hydrological cycles, rising temperatures, changing ecosystems, and increasing challenges for infrastructure, agriculture, and water resource management (Førland et al., 2002; SOU, 2007; Tietäväinen et al., 2010; Nikulin et al., 2011; Mikkonen et al., 2015; Grusson et al., 2021; Lind et al., 2023). However, addressing these issues requires localized, reliable, and high-resolution climate datasets that can capture both regional variations and microscale climate features well.

40 Traditional global climate models (GCMs), while valuable, often fail to offer the level of detail needed for regional or local-scale assessments. To fill this gap, various well-recognized gridded datasets such as the Climate Research Unit (CRU) dataset (Harris et al., 2020), the E-OBS database (Haylock et al., 2008; Cornes et al., 2018), the European Climate Assessment and Dataset (ECA&D) (Klein Tank et al., 2002; Klok and Klein Tank, 2009), the Global Precipitation Climatology Centre (GPCC) dataset (Yu et al., 2020), the HadGHCND dataset (Caesar et al.,
45 2006), ERA Interim (Dee et al., 2011), the ERA5 dataset (Hersbach et al., 2020), and CERRA (Schimanke et al., 2021) are widely available online and frequently used for climate impact assessment, climate adaptation and mitigation purposes. Each of these datasets has its strengths and limitations, and understanding these distinctions is crucial for selecting the most appropriate data for specific climate studies.

Among the climate datasets for the Nordic region, the Nordic Gridded Climate Dataset (NGCD) from Met Norway
50 (Lussana et al., 2018; Lussana et al., 2019) has emerged as a strong candidate for climate analysis. The NGCD covers Fennoscandia (Finland, Sweden, and Norway) at a horizontal resolution of 1 km, with data available from 1961 to the present. The dataset contains daily air temperature (mean, maximum, and minimum) and daily precipitation. There are two main constraints of this dataset: 1) it does not provide sub-daily information for the variables, and 2) the input data used to produce NGCD has low coverage of stations, which may result in
55 uncertainties, particularly in remote northern regions (Tveito and Lussana, 2018). Another potential candidate is data from the UERRA surface reanalysis, MESCAN-SURFEX (Soci et al., 2016; Bazile et al., 2017a; Le Moigne



et al., 2020). The spatial resolution of the MESCAN-SURFEX data is 5.5 km, with a time span from 1961 to 2018. This dataset provides analysis of daily accumulated precipitation and six-hourly analyses of air temperature, wind, and relative humidity, but it lacks maximum and minimum temperature data. Furthermore, MESCAN-SURFEX
60 has shown some quality issues with precipitation (Soci et al., 2016; Monteiro and Morin, 2023).

To address the discrepancies in existing gridded datasets for the Nordic regions, a high-resolution dataset called SMHIGridClim (Swedish Meteorology and Hydrology Institute Gridded Climatology) has been developed. The primary aim of this dataset is to provide high-quality, long-term climate information for Sweden. Additionally, it offers comprehensive climate data for regional analysis across neighbouring countries like Finland and Norway.
65 In this paper, a detailed overview of the SMHIGridClim dataset is provided to assist users in understanding its structure, features, variables, and potential applications for climate analysis in the Nordic regions.

SMHIGridClim is developed to meet the need for a climate reference dataset that offers high temporal resolution (sub-daily), fine spatial resolution (2.5 km horizontally), a long-time span (starting from 1961), key climate indicators (see below), and spatial coverage across Fennoscandia and the Baltic States. Above all, SMHIGridClim
70 is specifically designed for use in climate scenario services. It offers a reliable source of historical climate data, enabling researchers to investigate past climate conditions with greater precision and accuracy. Moreover, the dataset can be used to adjust the output of climate models to correct biases. In short, SMHIGridClim represents valuable data applicable across various sectors, including agriculture, forestry, hydrology, and urban planning, to improve climate-related decision-making at regional scales. The dataset has, for instance, been used in research
75 connecting people's health with the weather (Raza et al., 2024).

Optimal interpolation combines observations and gridded forecasts as the first guess (the initial state of the variables) to create a high-resolution gridded climatology dataset. The dataset covers Fennoscandia and the Baltic States during the time period 1961–2018 and includes the variables 2 m temperature (tas) and relative humidity (hurs) with 1-, 3-, and 6-hourly resolution (depending on the time period), along with daily precipitation (pr), snow
80 depth (snd), maximum (tasmax), and minimum (tasmin) temperature.

The structure of the paper is as follows. Section 2 presents the data included in the analysis, along with the tool for quality control. Section 3 describes the analysis method and provides an overview of the gridpp performance. Section 4 presents the results from the validation of SMHIGridClim, which are further discussed in Section 5, together with the conclusions. Acknowledgements are given in Section 6.



85 2 Data

The data used in the analysis consist of in-situ observations and gridded fields from numerical weather prediction (NWP) models. Figure 1 provides an overview of the processing steps and the variables included in SMHIGridClim. For near-surface humidity, the analysis is based on dew point temperature at 2 metres (Td2m) rather than relative humidity. This choice is motivated by the difficulty of analysing a variable with hard physical bounds, as is the case with relative humidity. Additionally, snow depth is not available from the UERRA dataset and was therefore derived from snow water equivalent and snow density.

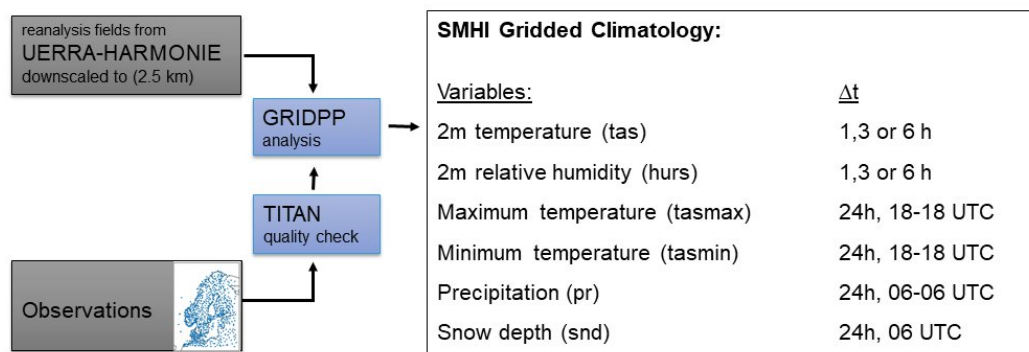


Figure 1. Overview of the processing steps of data for analysis with gridpp, and the produced variables in SMHIGridClim.

95 2.1 Observations

2.1.1 Observational data sets

Local in-situ observations were collected from the national meteorological institutes in Sweden, Norway and Finland, as well as from ECMWF's MARS archive. The Swedish observations were extracted from SMHI's Meteorological Observational Real-time Archive (MORA) database. Since SMHI has an open data policy, the data are freely available, and more information (in Swedish) can be found at: <https://www.smhi.se/data/utforskaren-oppna-data/>. Data from Norway were retrieved from the Frost archive at the Norwegian Meteorological Institute. The Frost archive contains historical weather and climate data that are also freely available: <https://frost.met.no>. Data from Finland were obtained from the Finnish Meteorological Institute's internal database, also freely available: <https://en.ilmatieteenlaitos.fi/open-data>.



105 During the early years of the SMHIGridClim period, only a few Td2m observations were available in the Norwegian national data. Therefore, Td2m was calculated from tas and hurs using Eq. (1):

$$hurs = 100 * \exp((17.625 * Td2m) / (243.04 + Td2m)) / \exp((17.625 * tas) / (243.04 + tas)), \quad (1)$$

where the unit for both tas and Td2m is °C. For all data streams, Td2m was checked to ensure it did not exceed the observed tas. If a Td2m value was higher than the corresponding tas + 5°C, it was set to missing. If it was between
110 tas and tas + 5°C, it was adjusted to match tas.

In addition to the national observations, data stored in BUFR format were extracted from ECMWF's MARS archive and used in the analysis. BUFR (Binary Universal Form for the Representation of meteorological data) is a binary data format maintained by WMO (World Meteorological Organisation). All available land surface data were retrieved as SYNOP station observations from the ECMWF's BUFR files. Variables extracted from the MARS
115 archive in BUFR-format include tas, Td2m and snd.

2.1.3 Observation density

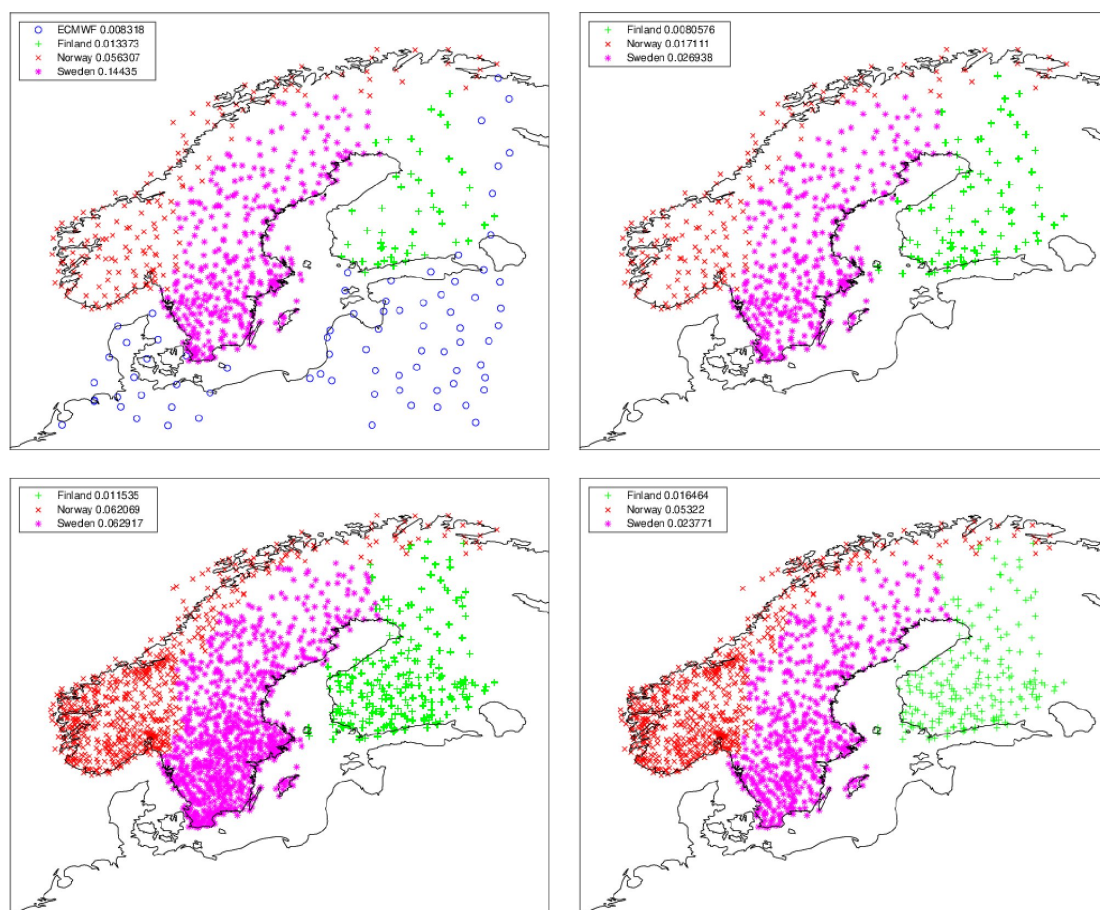
Observation density varies over both decadal and diurnal time scales, and it also differs depending on the observed variable.

Figure 2 shows examples of the spatial distribution of observations for tas, tasmax/tasmin, pr, and snd during a
120 month in 1965. In the early years of the SMHIGridClim period, ECMWF BUFR data were limited for tas and snd, making the national datasets particularly important. For observations of tasmin, tasmax, and pr, the national data are crucial, as BUFR data are not available at all during this early period. Across all datasets, the northern part of Scandinavia shows areas with sparse data coverage — notably in northern Sweden near the Norwegian border, and in northern Finland near the Swedish border. These areas of relatively low observation density are associated with
125 higher uncertainty in the analysis.

Figure 3 shows observation density on a decadal scale. There is a marked increase in the number of tas observations from 1995 onwards. This is primarily due to the expansion of automatic weather stations, which report at higher frequency — typically hourly. The increase in the number of tasmin observations reflects only the densification of the station network, as this variable is reported once per day. For all data streams, the number of pr observations
130 has declined from the 1980s onwards. The number of snd observations shows no clear trend for Swedish and Finnish data, while the Norwegian station density shows a distinct decline between 2000 and 2005.



The number of tas and Td2m observations during the day vary over time, as a consequence of observation frequency and the amount of digitalised data. A preliminary analysis showed that it is not meaningful to analyse more than



135

Figure 2. Observation density maps for of T2m (upper left), Tn (upper right), RR (lower left) and SD (lower right). Maps include data since July 1965 (February for SD) from different data sources. Observations represent those that are available for the whole month. The number of observations normalized by their corresponding representative areas, thus number of observations per km², are shown in the legend.

140

every 6th hour for the period 1961-1967, and every 3rd hour for the period 1968-1996. From 1997 and onward the network (mainly due to the introduction of the automatic stations) provides enough observations to allow an analysis for every hour of the day. However, the density of observations still varies considerable between the traditionally reporting hours (06, 12 and 18) and the intermediate ones.

145

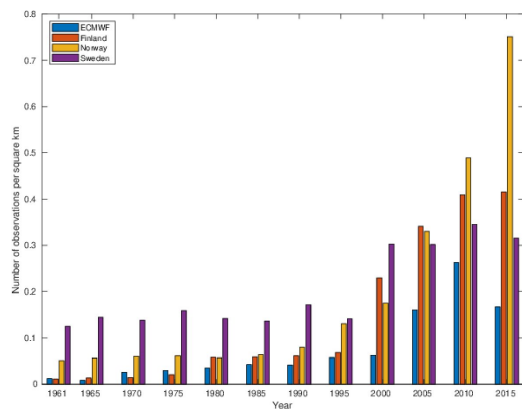
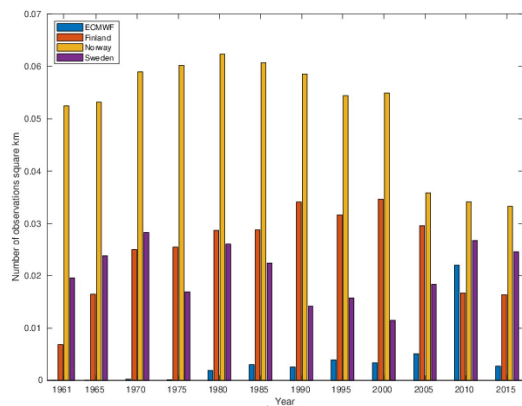
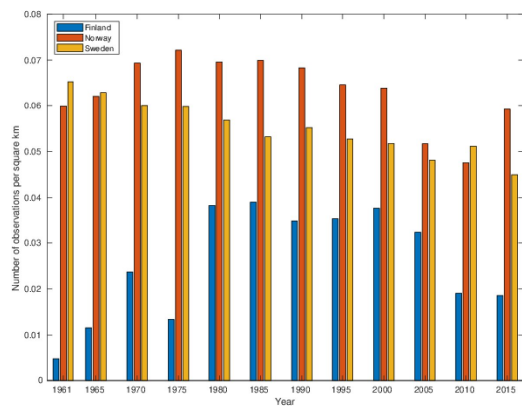
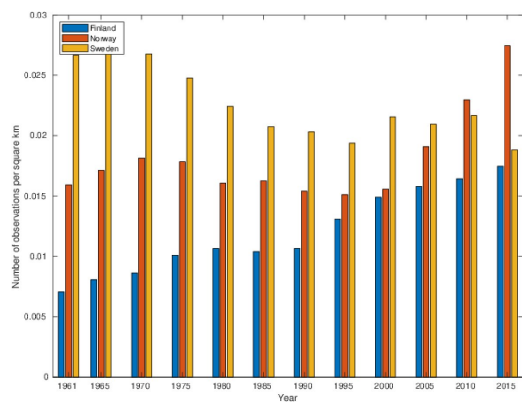


Figure 3 Observation density bar plots per year for (top to bottom) *tas* (July), *tasmin* (July), *pr* (July) and *snd* (February). The bars are colour coded with respect to data sources BUFR from ECMWF, Norway, Sweden, and Finland. The observations represent those that are available for the whole month taken into account that they are considered valid within specified limits. The numbers represent number of observations normalized by their corresponding representative areas, thus no obs per month per km².





2.2 Observation quality control

Observation quality control was carried out using the TITAN package (<https://github.com/metno/TITAN/wiki>), developed at Met Norway (Båserud et al., 2020). Note that TITAN has been replaced by a new package, titanlib
150 (<https://github.com/metno/titanlib/wiki>).

TITAN requires input data including station coordinates (latitude and longitude), station altitude, and the observation to be checked. All observations are assumed to be independent in time, as TITAN does not account for temporal correlations. The package offers several quality controls (QC) tests and configuration options (Båserud et al., 2020). The specific checks used in this study are summarised in **Table 1**. For further details on the TITAN
155 settings, refer to Andersson et al. (2021).

The TITAN outputs a Data Quality Control (DQC) code that indicates whether the observation is considered valid (DQC=0) or suspicious (DQC>0). Note that the isolated station check in TITAN was disabled in this study.

In addition to the checks performed by TITAN, a gross error check was applied using the first guess from the analysis. The first guess was interpolated to the observation locations using bilinear interpolation. For temperature
160 variables, the interpolation accounted for elevation differences between the model grid and the station location, using lapse rates of -0.0065 K/m for tas and -0.0017 K/m for Td2m. If the difference between the observation and the interpolated first guess exceeded three times the standard deviation of all differences, the observation was considered a gross error and was removed.

This gross error check was applied to all variables except for daily precipitation (pr), as precipitation fields can be
165 highly variable and spatially discontinuous. Applying the check to pr could lead to the erroneous removal of valid but spatially patchy observations (e.g., local showers not captured by the forecast model).

Table 1. The table presents the TITAN quality checks together with a short description. Options used in the present study, and the DQC number, where it is applicable, is also shown.

Quality checks	Information about the checks	Options in the present study	DQC
Digital Elevation Map (DEM) check	Check if the altitude specified for each observation agrees to the DEM within certain limits.	The allowed deviation is set to 300 m. The DEM check is applied to observations of tas, Td2m, tasmin and tasmax	5



Digital Elevation Map fill	To fill missing elevation data.	This option is applied to observations of pr and Sn,	-
Missing observations or meta data	If any of the input data includes Not a Number, the observation is flagged as missing data or metadata.	Applied to all data.	1
Plausibility range	If any observation is outside specific bounds, the observation is flagged as failing the plausibility test.	Applied to all data.	2
Buddy check	Compares the observations against the average of all neighbours in a square box centred on each observation.	Certain adjusted settings are used for observations of pr and snd.	4
Spatial consistency test	Evaluating the likelihood of an observation given the values observed by the neighbouring stations (Lussana et al., 2010).	It is used as the main quality test for tas, Td2m, tasmin and tasmax. The test is also used for pr and snd observations, although the thresholds are quite high which means that only extreme deviations are flagged.	5
Duplicates	To avoid duplicates in the analysis.	The threshold is set to 0.01 degrees apart and 100 m apart in altitude. The duplicates are removed before any other check in TITAN.	-

Refer to Andersson et al. (2021) for full documentation of TITAN settings.



170 2.3 Numerical weather prediction data

Forecasts from the UERRA-HARMONIE reanalysis (Copernicus Climate Change Service, 2019) were used as the basis for creating the first-guess fields in the SMHIGridClim analysis. Importantly, the analysis fields from UERRA-HARMONIE (available at 00, 06, 12, and 18 UTC) were not used as first guesses, as they include information from some of the observations included in the analysis.

175 For an overlapping time period (January 2016 to July 2019), the UERRA-HARMONIE fields were complemented with corresponding forecasts from the Nordic operational NWP system MEPS (Frogner et al., 2019). These forecasts, together with the UERRA-HARMONIE data (with a horizontal resolution of 11 km), were downscaled to the SMHIGridClim domain. The SMHIGridClim grid is defined as a subset of 823×567 points from the MEPS grid, with a horizontal resolution of 2.5 km. The spatial coverage of UERRA-HARMONIE, MEPS, and
180 SMHIGridClim is shown in Figure 4. The downscaling process is described in detail in Section 3.1.

Model areas. Red: UERRA, Blue: MEPS, Green: SweGridClim

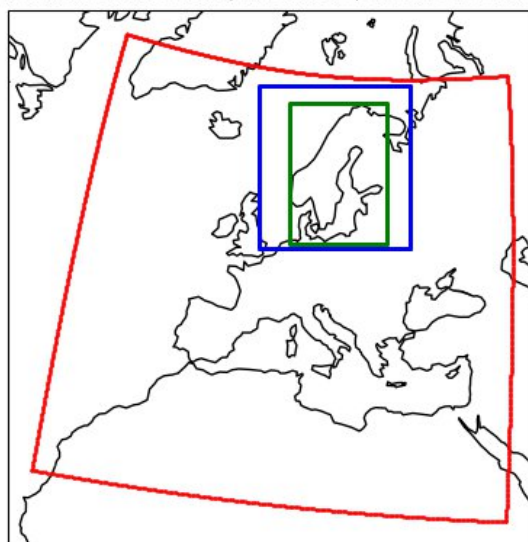


Figure 4. The areas covered by the different model grids of datasets in this paper. Red: Uerra-Harmonie at 11 km. Blue: MEPS at 2.5 km. Green: SMHIGridClim at 2.5 km (subset of the MEPS grid).

185



190 Table 2 provides an overview of the forecast cycles and lead times used for each variable in the SMHIGridClim
 dataset. For tas and Td2m, MEPS data were retrieved as 6-hour forecasts: 00+06, 06+06, 12+06, and 18+06. No
 direct MEPS fields were available for tasmin or tasmax. Instead, relationships based on tas at midpoints of the
 195 tasmin and tasmax time windows were used, as shown in Table 2. Precipitation (pr) was derived from a combination
 of accumulation periods, while snow depth (snd) was assumed to be measured at 06 UTC and was therefore based
 on the 00+06 forecast. However, snd is not available as a model output from either UERRA-HARMONIE or MEPS
 and was derived from snow water equivalent (SWE) and snow density (rho). Since snow density is not available
 from MEPS, only SWE was downscaled from UERRA-HARMONIE. This derivation is further described in
 Section 3.1.

Table 2. Forecast cycles and lengths of the UERRA-HARMONIE fields for the different entities in the SMHIGridClim data set (SWE is snow water equivalent, and rho is snow density).

Variable	Forecast cycle 00	Forecast cycle 06	Forecast cycle 12	Forecast cycle 18
tas, hurs	00+01	06+01	12+01	18+01
	00+02	06+02	12+02	18+02
	00+03	06+03	12+03	18+03
	00+04	06+04	12+04	18+04
	00+05	06+05	12+05	18+05
	00+06	06+06	12+06	18+06
tasmin/tasmax 18-18	00+03-04		12+03-04	
	00+04-05		12+04-05	
	00+05-06		12+05-06	
	00+06-09		12+06-09	
	00+09-12		12+09-12	
	00+12-15		12+12-15	
pr 06-06	00+06		12+06	
	00+18		12+18	
SWE, rho	00+06			



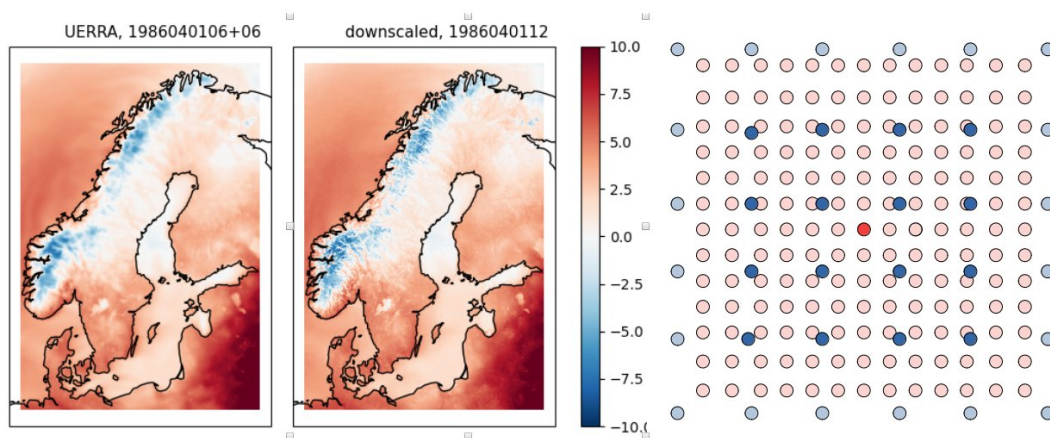
3 Methods

200 3.1 Downscaling the first guess

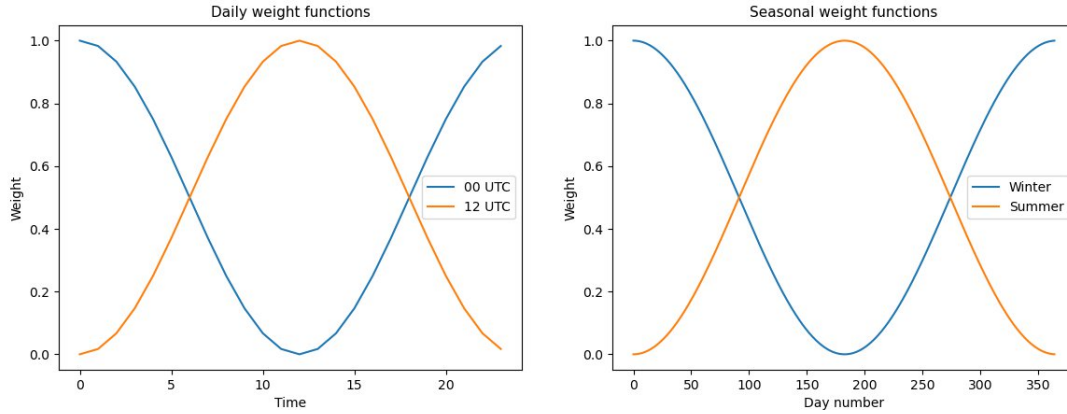
Data from the overlapping MEPS and UERRA-HARMONIE period (see Sect. 2.3) were used to establish a relationship based on linear least squares regression. The regression was performed between a given point on the SMHIGridClim domain (2.5 km horizontal resolution, derived from the MEPS grid) and its surrounding 4×4 neighbouring points in the UERRA-HARMONIE grid (11 km resolution).

205 Figure 5 shows an example of tas from UERRA-HARMONIE interpolated to the 2.5 km grid and the corresponding downscaled fields. The downscaled tas demonstrates finer spatial structure, particularly in mountainous regions of Norway and Sweden. The right-hand panel of Fig. 5 illustrates how each grid point in the 2.5 km grid is linked to its 16 nearest neighbours in the 11 km UERRA-HARMONIE grid.

For tas and Td2m, four separate weighted regressions were calculated — for day and night (00 and 12 UTC), and
210 for mid-winter and mid-summer, respectively. Final weights, combining diurnal and seasonal variation, were computed using squared cosine functions centered at 00 and 12 UTC, and at day numbers 0 and 183. The weighting functions are illustrated in Figure 6. This results in a set of 4×16 regression parameters for each grid point and variable.



215 *Figure 5. Example illustrating the downscaling of temperature from UERRA to the 2.5 km grid used in SMHIGridClim. Left: Original UERRA field interpolated to the SMHIGridClim grid (unit: degrees Celsius). Middle: Downscaled field. Right: Schematic illustration of how a point (dark red) in the 2.5 km grid is associated with its 4x4 neighbourhood (dark blue dots) in the 11 km UERRA grid.*



220

Figure 6. Weighting functions for the downscaling parameters. Left: Daily weighing functions for 00 and 12 UTC parameters. Right: Weighing functions for the seasonal parameters at day number 0 (winter) and 183 (summer).

225 For *tasmin* and *tasmax*, no separate regressions were conducted. Instead, the relationships derived for *tas* were applied to each of the 12 hours throughout the day (see Table 2). Weights for *pr* downscaling were derived based on seasonal variation only, with no diurnal dependence. In addition, a non-negative least squares approach was applied to ensure all downscaled values were non-negative.

230 The same weighting functions used to derive regression parameters during the overlapping time period were applied to full UERRA-HARMONIE time series, allowing parameter interpolation for any given day and time:

$$wd_{00} = \cos\left(\frac{(hr - 0)}{2/24} (2\pi)\right)^2 \quad (2)$$

$$wd_{12} = \cos\left(\frac{(hr - 12)}{2/24} * (2\pi)\right)^2 \quad (3)$$

$$wy_w = \cos\left(\frac{(dn - 0)}{2/365.25} * (2\pi)\right)^2 \quad (4)$$

$$wy_s = \cos\left(\frac{(dn - 365.25)}{2/365.25} * (2\pi)\right)^2 \quad (5)$$

235 Where *hr* is the analysis hour, *dn* is the day number of the year, wd_{00} and wd_{12} are diurnal weights, and wy_w and wy_s are seasonal weights. These weights are then used in a linear combination of the regression parameters associated with 00 and 12 UTC, and with winter and summer, respectively:

$$p = wd_{00}(p_{00w} * wy_w + p_{00s} * wy_s) + wd_{12}(p_{12w} * wy_w + p_{12s} * wy_s) \quad (6)$$



Where p is the combined regression parameter used for downscaling.

240 For tasmin and tasmax, each of the 12 sub-daily intervals (Table 2) was downscaled individually, using the midpoint of each interval to determine the appropriate weighting.

Downscaling of daily snow water equivalent (SWE) was performed using constant weights and involved several steps. First, SWE was downscaled from UERRA-HARMONIE using the regression-based approach described above. Subsequently, snow depth (snd) was estimated by dividing the downscaled SWE by the snow density
245 interpolated from UERRA-HARMONIE to the SMHIGridClim grid. To correct for systematic differences between the distributions of downscaled and observed snow depth, a bias correction was applied using quantile mapping (QM). This procedure included imposing an upper limit of 10 m on the downscaled snow depth, reflecting the maximum observed values, followed by sorting the observed and downscaled snow depth data to establish a lookup table with 5000 pairs evenly distributed between 0 and 10 meters. The QM method then linearly interpolated
250 between these points to map the downscaled snow depth distribution onto the observed distribution. Quantile mapping has been shown to effectively correct systematic errors in precipitation-related variables (Panofsky and Brier, 1968; Themeßl et al., 2012).

3.2 Analysis with gridpp

The analysis was done using the open source software gridpp developed by the Norwegian Meteorological Institute
255 (<https://github.com/metno/gridpp>). Specifically, the python library version of gridpp was employed, which offers functions for performing analyses using optimal interpolation (OI). This technique statically combines observations and gridded forecasts (referred to as the first guess) in an optimal way (Gandin, 1965). In addition to OI, the library includes functions for operations such as bi-linear interpolation and diagnosing calculation of meteorological entities.

260 To conduct an OI analysis, information about the spatial covariances of both the first guess and the observations is required. In gridpp, these covariances are represented by an error variance ratio and a correlation (or structure) function, with the latter capable of being modelled using various approaches.

For the SMHIGridClim analysis, we apply the "optimal_interpolation" function from gridpp, with the argument max_points set to zero, thereby allowing all available observations within the localization zone to be considered
265 without restriction. To define the localization zone and its associated correlation structure, we employ the flexible BarnesStructure formulation (Barnes, 1973). This structure accepts four arguments: (1) the horizontal



decorrelation length scale (in metres), (2) the vertical decorrelation length scale (in metres), (3) the decorrelation length scale based on differences in land area fraction (unitless), and (4) the maximum influence radius of an observation (in metres), also referred to as the localization radius. For SMHIGridClim, the fourth argument was
270 left unspecified, invoking the default setting; 3.64 times the horizontal decorrelation length.

A cross-validation procedure was conducted to determine suitable parameter values for the error variance, the ratio between first guess and observation error variances, and the parameters governing the structure function. This procedure is implemented within gridpp, which performs the analysis using a “leave-one-out” cross-validation approach. Specifically, for each observation point, the corresponding observation is excluded from the OI analysis
275 to estimate the error at that location. Although this error estimate may not fully represent the spatial scale of the OI analysis, it provides valuable independent information on how well the analysis fits the observations.

The optimal parameters of the structure function depend on the observation density, which varies over time. Consequently, optimal parameters were derived for selected years (1965, 1975, 1985, 1995, 2005, and 2015) within the 1961–2018 period. For the remaining years, parameters were obtained through spline interpolation, with the
280 values for 1965 and 2015 applied to the years 1961–1964 and 2016–2018, respectively. Separate parameter sets were assigned for night and day as well as for winter and summer, employing the same weighting functions (wf) as used in the downscaling step, augmented with a 10-year wide weighting window around each reference year:

$$wf = \left(\cos\left(\frac{yr - yr_k}{2/20 * (2\pi)}\right)^2 \right) \quad (7)$$

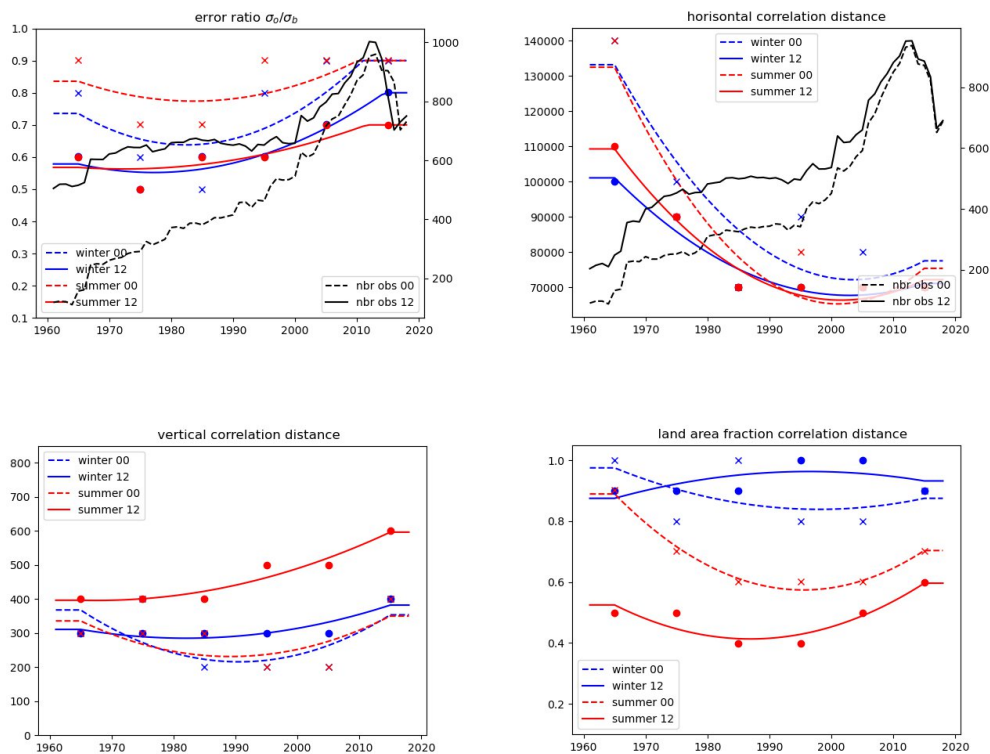
where yr corresponds to the year for which the calculation will be carried out, and $yr_k = (1965, 1975, 1985, 1995,$
285 $2015)$.

For any given year and date within the time period, parameter values were then smoothly interpolated using splines. Allowing temporal variation in the parameters improves the performance of the analysis at different times, albeit at the cost of violating strict homogeneity assumptions. However, the influence of this temporal variability is small relative to the larger effects of changing observation density over time.

290 The final optimized gridpp parameters used for the temperature analysis are illustrated in Figure 7, alongside the average number of observations. Similar procedures were followed for tasmin, tasmax, and Td2m. For daily precipitation and snow depth, the optimization yielded relatively constant parameter values across years and seasons; therefore, fixed values were used for these variables, as summarized in Table 3.



As described in Section 3.1, the analysis was performed using the downscaled fields as the first guess. One
 295 exception was relative humidity (hurs), which was not directly analyzed with gridpp. Instead, it was diagnosed
 using the gridpp.relative_humidity function, using the analyzed tas and Td2m fields as inputs. This approach was
 chosen because the error distributions of tas and Td2m fit a normal distribution better than those of hurs, which is
 constrained between 0 and 100%, complicating error estimations.



300

Figure 7 Time interpolation of optimized gridpp parameters for 2m temperature. Black lines show the mean number of observations per analysis date on the axis to the right. Top left: Error variance ratio (unitless). Top right: Horizontal correlation (unit: m). Bottom left: Vertical correlation (unit: m). Bottom right: Land area fraction correlation (unitless).

305



Table 3. Optimal gridpp parameters for the analysis of daily precipitation.

	Error variance ratio	Horizontal distance	Vertical distance	Land area fraction
precip	0.30	43 km	1800 m	0.0
snowd	0.90	35 km	350 m	0.55

4 Results

310 This section describes the result from the analysis with gridpp as well as from the data processing steps. In section
4.1 an overview of the final climatology data is presented in terms of difference maps between the period 1961-
1990 and 1991-2018. The following sections 4.2, 4.3 and 4.4 illustrates the results of the different processing steps
in the analysis, starting with cross validation of the dataset with observations, followed by the result of the
downscaling of UERRA fields, and the analysis increments from interpolation with gridpp.

4.1 Climatologies

315 Figure 8 shows the resulting climatologies from SMHI GridClim in terms of maps showing the difference between
the period 1991-2018 and the standard reference period 1961-1990 according to World Meteorological
Organization (WMO). This gives a view of how the dataset represents changes in the variables over time. For
temperature related parameters tas, Td2m, tasmin and tasmax, increase is seen over almost the entire region as
expected due to climate change. This increase is largest for the daily minimum temperature, with up to two degrees.

320 For relative humidity the result is patchier and the differences between the climate periods are generally small,
indicating no clear trend. Precipitation on the other hand generally shows an increase between the two periods.
This increase is most pronounced in the south-east part of Norway, where the yearly precipitation is already at its
highest. Also, in Sweden the precipitation shows a noticeable increase in the west coast region.

The snow depth generally shows a decrease, as can be expected from a warmer climate, except in northern Finland
325 and in some small areas in the Norwegian mountains and northern Sweden.



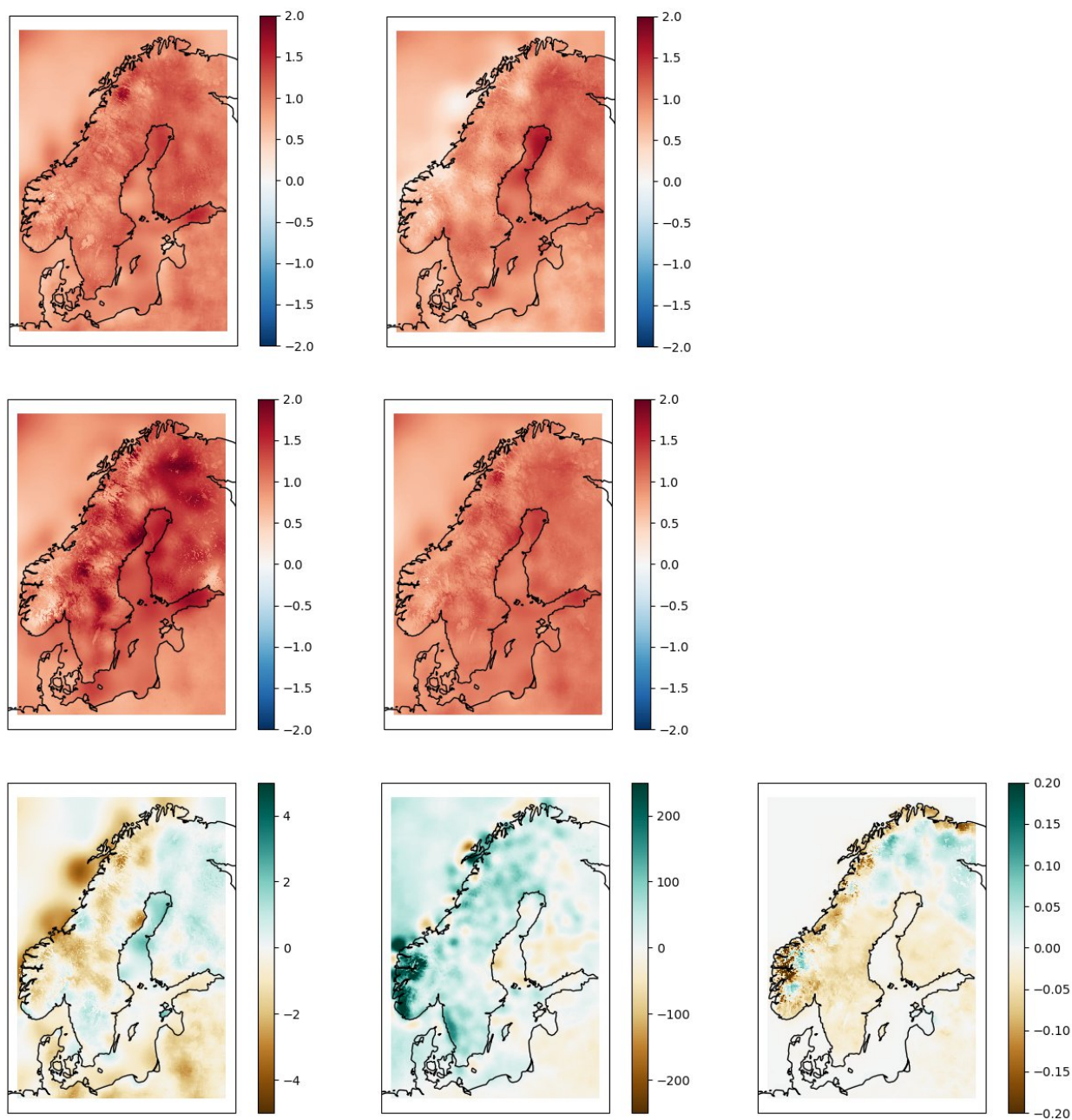
Note that there are some isolated points standing out in the difference maps, clearly seen for the relative humidity and the precipitation. They are mainly located in coastal regions, especially along the Norwegian coast, for example around Lofoten. The reason for these deviations is that the contrast between land and sea is not represented by the scale of the grid used for the analysis. Thus, stations located in coastal areas, exhibit an influence on sea-covered area giving values that are less realistic. However, over Sweden, which is the focus area of this analysis, the fields look rather smooth.

4.5 Cross validation

In order to obtain an estimate of the analysis error, cross validation between observations and the data fields was done at each analysis time step for any given analysis. Therefore, cross validation results are given for the original UERRA fields, the downscaled field used for first guess, and the resulting analysed fields. The exception was for hours that was diagnosed from dew point temperature, thus cross validation was done also for dew point temperature. The cross-validation results for 12 UTC for all analysed parameters is shown in Fig. 9. Plots for other hours can be found in the dataset technical report (Andersson et al., 2021)

With a few exceptions, both the downscaling of UERRA fields and the analysis with gridpp improved the statistics for most parameters, in terms of decreased standard deviation, mean difference and RMSE.

A limitation that was that temperature fields from both UERRA and MEPS both were shown to have too low maximum temperatures, and too high minimum temperatures, compared to the observations (panel d and e). In addition, MEPS in general had warmer temperatures than UERRA, which worsened the situation for low temperatures as the downscaling were done under the assumption that the performance of the MEPS forecast is superior to that of the UERRA forecast. Below some more details about the results are discussed.



350 *Figure 8. Differences between climatologies for the time periods 1991-2018 and 1961-1990. Top left: hourly mean T2m. Top right: Hourly mean Td2m. Middle left: Daily mean Tn. Middle right: Daily mean Tx. Bottom left: Hourly mean rh2m. Bottom middle: Yearly mean RR. Bottom right: Daily mean Sn.*



For **two-meter temperature (Fig. 9a)**, a negative bias of the UERRA forecast valid at 12 UTC means that the model fields are generally too cold. Here, the downscaling improves on both the bias and the standard deviation. 355 As a result, the total error in terms of the RMSE is also improved by the downscaling. The statistics for other hours follow a similar pattern, with the exception that at 00 UTC the downscaling actually increases an already positive bias even more (not shown).

Furthermore, the first guess entering the optimal interpolation show a positive bias that seems to grow towards the end of the time period. There is however a slight improvement in the standard deviation of the UERRA data over 360 time. The added number of observations towards the end of the period does not lead to any significant improvement on the analysis error. An increasing bias in the first guess are also seen for several other parameters, the reason for this has not been investigated further.

For the **dew point temperature (Fig. 9b)**, the downscaling improves the standard deviation but does not significantly change the systematic overestimation (positive bias) of Td2m in the UERRA forecasts valid at 12 365 UTC. During the night (not shown here) the downscaling helps improving a negative bias at the end of the time period, although it overcompensates somewhat in the early years.

For the **relative humidity (Fig. 9c)**, which was calculated from the downscaling of tas and Td2m, thus no observations of hurs enter the analysis. Instead, the comparison is done to relative humidity values calculated from co-located observations of tas and Td2m.

370 Here, although the downscaling clearly adds value compared to the UERRA forecasts, the analysis cannot fully compensate for the bias in the first guess and one can see a small increasing trend also in the bias of the analysis.

For the daily **minimum temperature (Fig. 9d)**, the downscaling results in only slightly lower standard deviation and hardly any difference in rms. At the same time the positive bias is increasing. Although the downscaling did not improve the fields for first guess, the rms did not increase notably, and the analysis compensates for this in the 375 final results.

Also, there is a trend towards lower RMSE values over time for the first guess for minimum temperature. This trend is not carried over to the analysis to the same extent, even though it should be further strengthened by the increase in observations towards the end of the period.

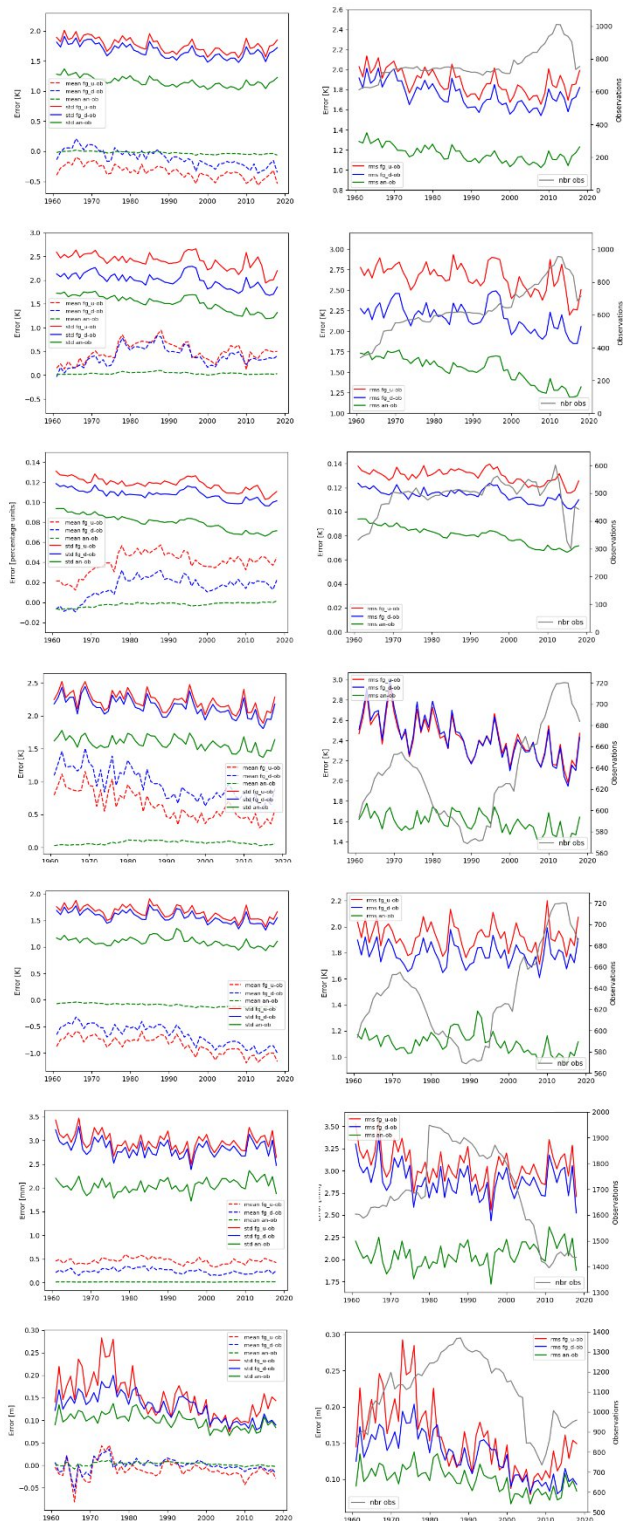


Figure 9. Error statistics for all analysed parameters at 12 UTC. Left: bias (dashed lines) and standard deviations (solid lines). Right: RMSE and number of observations. Red: UERRA, blue: downscaled, green: analysis.



For the daily **maximum temperature (Fig. 9e)**, the downscaling procedure results in a small improvement, both with respect to bias and standard deviation. The dip in the number of available observations around the 1980s and 1990s seems to be reflected in the RMSE of the analysis. Also, the trend towards lower RMSE values, as was seen for the daily minimum, is not as pronounced for the daily maximum.

385 Error statistics for **the daily precipitation (Fig. 9f)** generally show the expected improvement, a bias close to zero and a clear improvement on top of the first guess. The number of observations peaks during the 1980s and 1990s, this coincides with an improved RMSE for the first guess but is not seen clearly in the RMSE of the analysis.

Finally, for **the daily snow cover (Fig. 9g)**, the downscaling of the UERRA forecasts most of the time results in lower standard deviation as well as a reduction in bias.

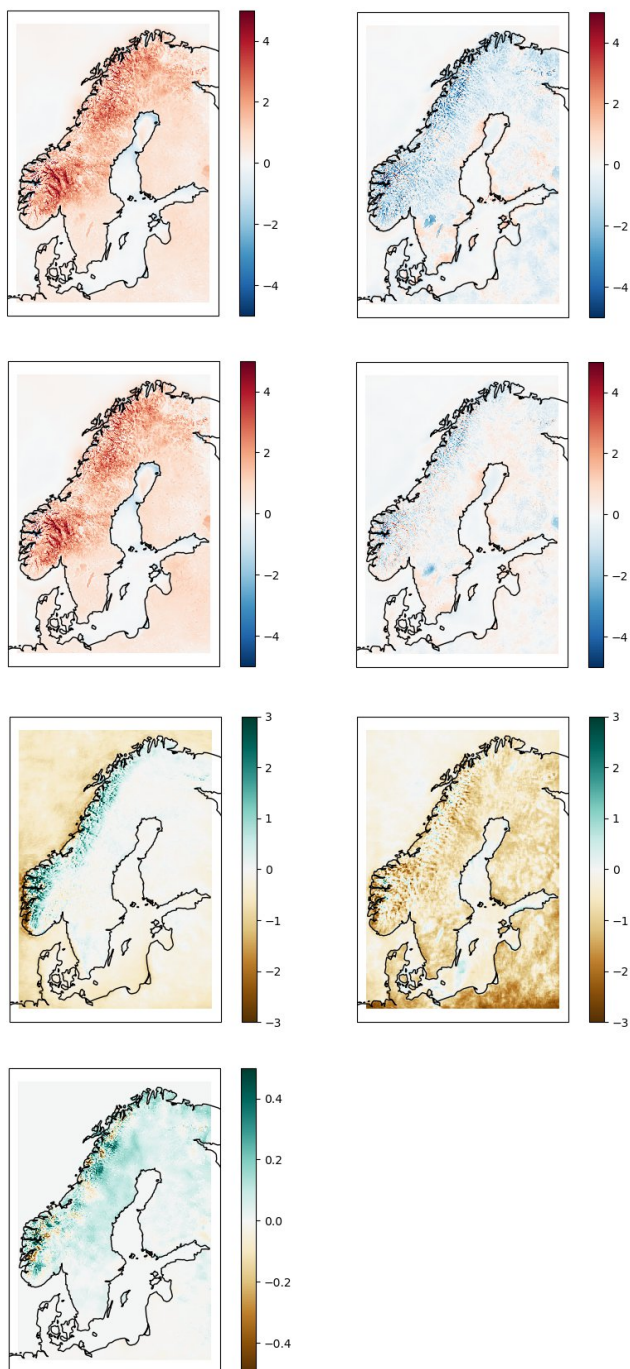
390 There is no clear connection between the error in the first guess and the yearly mean snow depth (not shown), nor with its 95:th percentile. The reason for the large errors in the UERRA snow fields during the 1970s has not been studied. There is no clear connection between the number of observations and the RMSE of the analysis. The analysis of daily snow cover shows almost zero bias and show added value from the first guess, at least during the first and last 15 years.

395 **4.3 Spatial structures of downscaling**

In addition to the cross validation results presented in section 4.2, the spatial behaviour of the processing steps was investigated by difference maps. For the difference maps showing the effect of the downscaling of UERRA, the fields first had to be interpolated to the SMHIGridClim grid using bi-linear interpolation. The downscaling procedure results in fields that fit the patterns in the corresponding MEPS fields during the years 2016 - 2018. The
400 assumption for the downscaling is that the performance of the MEPS forecast is superior to that of the UERRA forecast.

In Fig. 10, examples of the downscaling effect for one summer month, winter month and 12 UTC and 00 UTC are shown for two-meter temperature and for daily precipitation.

405 For two-meter temperature, it was shown earlier, in the cross-validation results, that the downscaling helped to reduce the negative bias in temperatures in UERRA. Looking into the downscaling in more details, in the winter (represented by January) the downscaling results in higher temperatures, both during night and day (Fig. 10). In the summer (July) on the other hand, it is the other way around, with the downscaling mostly producing colder temperatures, especially in the mountains during the day.



410 *Figure 10. Mean differences between T2m and RR from the downscaled and original UERRA fields respectively (unit: K). Top left: January 12 UTC. Top right: July 12 UTC. Bottom left: January 00 UTC. Bottom right: July 12 UTC.*



Note that the downscaling makes the two largest lakes in Sweden, Vänern and Vättern, slightly warmer during
415 winter and noticeably colder during summer.

During the winter the downscaling intensifies the precipitation in the mountains. For the summer period, the
downscaling instead results in a general decrease in the daily precipitation. For snow depth, downscaling increases
the depth for most places in the analysed area.

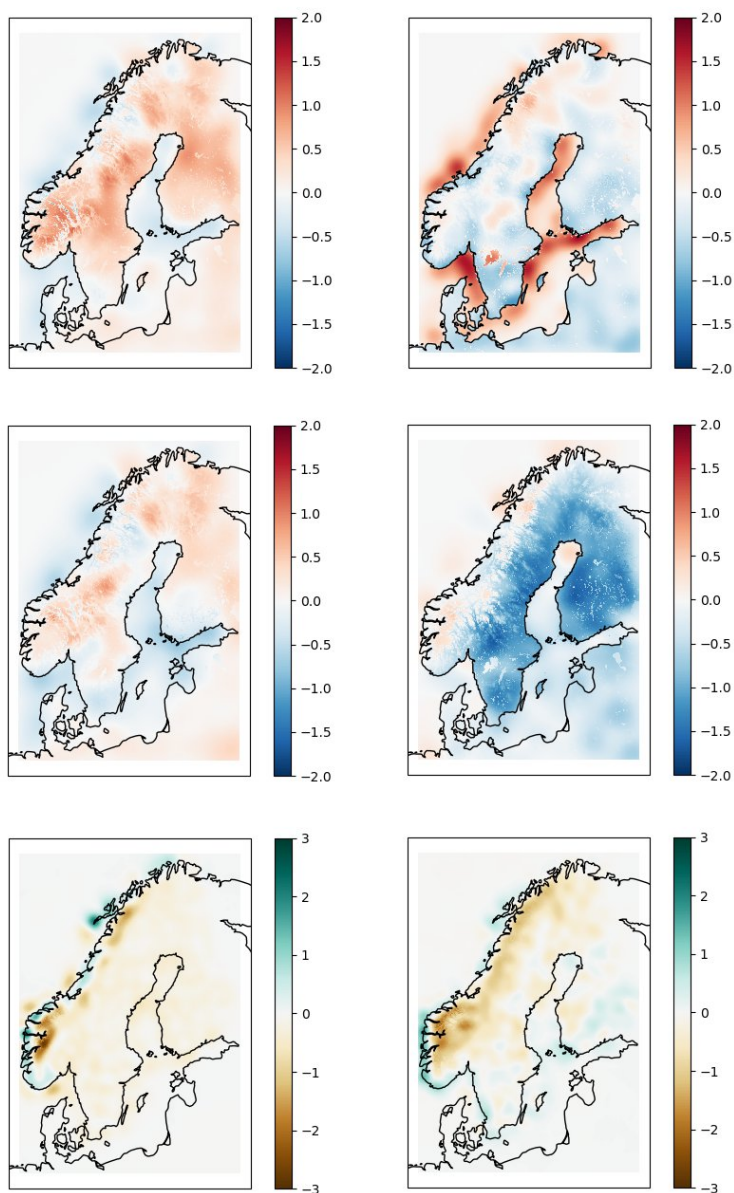
4.4 Spatial structures of analysis increments

420 Analysis increments are here shown as the difference between the analysis and the first guess, given by the
downscaled UERRA fields. Thus, they show the influence of the interpolation with gridpp. Note that this means
that positive values in the maps indicate that the first guess was too low and vice versa for negative values. Ideally
the distribution of the analysis increments should follow a normal distribution with zero mean.

425 Again, using tas as example, during the winter noon the analysis results in a systematic increase of the temperature
while it is the other way around during the summer night.

This can be compared to the differences between the downscaled and original UERRA fields shown in Fig. 11. The
downscaling resulted in warmer fields during the winter days but not warm enough to fit the observations. For the
summer night the downscaling was rather neutral indicating that both MEPS and UERRA have a positive bias for
that period. For minimum and maximum temperatures (not shown), the analysis changes the maximum to be
430 warmer and the minimum to be colder than what is suggested by the first guess. As discussed earlier for the cross-
validation results (Fig. 9), this shift is compensating for the downscaling towards the opposite direction in
temperature caused by the MEPS model, in order to fit the first guess to the observations.

The analysis increments for the daily precipitation show in general small changes but indicate that the first guess
has too much precipitation, especially in the Norwegian mountain regions. During summer, the first guess has too
435 little precipitation along the south-west Norwegian coast and there is also a slight tendency that the first guess
underestimates the precipitation along the Swedish west coast during the summer season.



440 *Figure 11. Mean analysis increments for T2m [°C] and RR [mm]. Top left: T2m January 12 UTC. Top right: T2m
July 12 UTC. Middle left: T2m January 00 UTC. Middle right: T2m July 00 UTC. Bottom left: RR, daily January.
Bottom right: RR daily, July*



5 Data availability

The SMHIGridClim dataset for the years 1961–2018 is available at <https://doi.org/10.5281/zenodo.845733> (Andersson et al., 2025). Work to extend the dataset to present day is currently being performed at SMHI.

6 Discussion and conclusions

SMHIGridClim was further evaluated by comparing cross validation results for SMHIGridClim with values found in the literature for two comparable datasets from the Nordic neighbour institutes Finland and Norway. The cross-validation results are mostly similar, especially SMHIGridClim and seNorge (Lussana et al., 2019 and Lussana et al., 2018). FMI_ClimGrid (Aalto et al., 2016) shows slightly better performance for the available variables in this dataset, which might be explained by more challenging topography to be represented for the Swedish and Norwegian datasets. Thus, SMHIGridClim provides a high-resolution gridded dataset, with a quality on par with similar datasets from other institutes.

In addition to the listed datasets, there are many well-known widely used reanalysis data, such as ERA5 (Hersbach et al., 2020) and CERRA (Schimanke et al., 2021). However, it is difficult to do a valid comparison as there exists no cross validation results. Also, the resolution of these datasets are many times coarser than in SMHIGridClim (~31 km and 5,5 km respectively).

Table 4. Mean RMSE for tas (hourly), tasmin, tasmax in kelvin (K), pr in mm, and snd in cm for three Nordic gridded datasets.

	tas (K)	tasmin winter (K)	tasmin summer (K)	tasmax winter (K)	tasmax summer (K)	pr (mm)	snd (cm)
SMHIGridClim	1.2 - 1.5	1.4 - 1.8		1.0 - 1.2		ca 2	11
seNorge2.0/2018	1.0 - 1.4	2.0 - 4.0	1.5 - 1.8	1.0 - 2.5	1.0 - 1.5	2 - 6	NA
FMI_ClimGrid	NA	1.0 - 1.7		0.5 - 0.8		0.4 - 1.5	6.3



465 A number of things should be kept in mind using this kind of modelled climatological data. Although the horizontal resolution of SMHI GridClim is 2.5 km, the effective resolution is larger due to the underlying model fields. With effective resolution we mean the resolution that has actual meaningful information. For MEPS at 2.5 km the effective resolution is likely about a magnitude larger. Due to the nature of numerical solutions and parametrizations, the model effective resolution degrades

to several grid spacings (Abdalla et al., 2013). This also affect the result of the evaluation of analysis increments as comparison was not done at its actual effective resolution.

470 Although SMHIGridClim is produced to be a high-resolution climate dataset, it is not appropriate to use for detailed studies of trends as it suffers from inhomogeneity. The dataset is based on UERRA reanalysis topped with observations. UERRA is based on a frozen model system which means that it does not change over time, but the observations show large variations in frequency and density and sometimes data quality. Furthermore, the parameters used in the analysis with gridpp was allowed to change in order to adapt to the observations available
475 over time. This could introduce false trends in data. To minimise this influence, one could have limited the analysis to only include long-term observations, but this would dramatically have limited the information available for the overall analysis, and therefore the quality.

The changing observation network leads to variation in data quality over time. In general, there are more observations available during the 6 hourly cycles: 06, 12, 18 and 24, followed by the 3 hourly: 06, 09, 12, 15, 18,
480 21 and 24, followed by the hourly. Also, there are less observations back in time. However, there are deviations from this so the observation density should be checked to conclude how it affects a specific study with regards to time period and region of interest. The amount of available observations differs widely over the analysed region, and the analysis is only truly valid for Sweden, Finland and Norway where national data was provided. Results are probably most reliable for Sweden where we had the best knowledge of observation quality, and less problems
485 with steep topography and fractal coastlines like in Norway. Over water surfaces, and some land regions, the analysis contains no observations, and therefore based on the downscaled version of the UERRA reanalysis only.

Catching extreme events in the dataset is also challenging. Although downscaling is done at an hourly basis, the underlying data field from UERRA has a rather coarse resolution of 11 km. Also, the downscaling is static at 00 and 12 UTC and is based on linear regression, thus it strives towards the best fit with the mean error as target. For
490 extreme precipitation also, the fact that optimal interpolation is based on a normal distribution is problematic



because this will not be representative for large precipitation events. Furthermore, there is different probability for the cases having precipitation or not to occur, and having precipitation with heavy rain/snow fall. The result is that precipitation is smeared out, and extreme events not well represented. Thus, these occasions should in the future be handled separately in the analysis with gridpp to improve the result.

495 There is ongoing work to develop SMHIGridClim. The development includes a switch to titanlib instead of TITAN, adding wind speed as a new variable, and switch the first guess to CERRA (Schimanke et al., 2021) instead of its predecessor UERRA. CERRA has the same domain as UERRA, although the horizontal resolution is 5.5 km instead of 11 km. At present CERRA is available for the period 1984 to 2023, however, there is ongoing work to extend the data set from 1961 to present day including operational updates. There is also a plan to include
500 observations from Denmark, Estonia, Latvia, and Lithuania which has been collected. Furthermore, a more thoroughly comparison between different gridded data sets would be of interest.

7 Author contributions

SA organized the project and wrote the manuscript. MN organized the project and wrote the manuscript. TL
505 downscaled the original UERRA fields, and performed the analysis with gridpp. PS preprocessed observation data and performed the quality control with the TITAN software. SS fetched observation data from different data sources and meteorological institutes. MZ helped with evaluation and wrote the manuscript. LB contributed as the initiator of the study and with expertise. All authors contributed to the manuscript writing.

8 Acknowledgements

We acknowledge Mariken Homleid (MetNorway) and Viivi Kallio-Myers (FMI) for providing observational
510 datasets and Cristian Lussana (MetNorway) for support with TITAN.

References

Aalto, J., Pirinen, P., and Jylhä, K.: New gridded daily climatology of Finland: Permutation-based uncertainty estimates and temporal trends in climate, *J. Geophys. Res. Atmos.*, 121, 3807–3823, <https://doi.org/10.1002/2015JD024651>, 2016.



- 515 Abdalla, S., Isaksen, L., Janssen, P.A.E.M., and Wedi, N.: Effective spectral resolution of ECMWF atmospheric forecast models, *ECMWF Newsletter*, 137, 19–22, <https://doi.org/10.21957/rue4o7ac>, 2013.
- Andersson, S., Barring, L., Landelius, T., Samuelsson, P., and Schimanke, S.: SMHI Gridded Climatology, Swedish Meteorological and Hydrological Institute (SMHI), <https://urn.kb.se/resolve?urn=urn:nbn:se:smhi:diva-6192>, 61 pp., 2021.
- 520 Andersson, S., Norman, M., Landelius, T., Samuelsson, P., Schimanke S., Zahid M., Barring, L.: SMHIGridClim, 2.5 km resolution gridded climatology of Fennoscandia, Harvard Dataverse [dataset], <https://doi.org/10.7910/DVN/ZFZL6K>, 2025.
- Barnes, S.L.: Mesoscale objective map analysis using weighted time series observations, NOAA Tech. Memo. ERL NSSL-62, 60 pp., <https://repository.library.noaa.gov/view/noaa/17647>, 1973.
- 525 Båserud, L., Lussana, C., Nipen, T.N., Seierstad, I.A., Oram, L., and Aspelien, T.: TITAN automatic spatial quality control of meteorological in-situ observations, *Adv. Sci. Res.*, 17, 153–163, <https://doi.org/10.5194/asr-17-153-2020>, 2020.
- Bazile, E., Abida, R., Verelle, A., Le Moigne, P., and Szczypta, C.: Report for the 55 years MESCAN-SURFEX re-analysis, Copernicus Climate Change Service,
530 <https://uerra.eu/component/dpattachments/?task=attachment.download&id=399>, 2017.
- Brohan, P., Kennedy, J.J., Harris, I., Tett, S.F.B., and Jones, P.D.: Uncertainty estimates in regional and global observed temperature changes: A new data set from 1850, *J. Geophys. Res.*, 111, D12106, <https://doi.org/10.1029/2005JD006548>, 2006.
- Caesar, J., Alexander, L., and Vose, R.: Large-scale changes in observed daily maximum and minimum
535 temperatures: Creation and analysis of a new gridded data set, *J. Geophys. Res.*, 111, D05101, <https://doi.org/10.1029/2005JD006280>, 2006.
- Cornes, R.C., van der Schrier, G., van den Besselaar, E.J.M., and Jones, P.D.: An ensemble version of the E-OBS temperature and precipitation data sets, *J. Geophys. Res. Atmos.*, 123, 9391–9409, <https://doi.org/10.1029/2017JD028200>, 2018.



- 540 Dee, D.P., Uppala, S.M., Simmons, A.J., Berrisford, P., Poli, P., Kobayashi, S., Andrae, U., Balmaseda, M.A., Balsamo, G., Bauer, P., Bechtold, P., Beljaars, A.C.M., van de Berg, L., Bidlot, J., Bormann, N., Delsol, C., Dragani, R., Fuentes, M., Geer, A.J., Haimberger, L., Healy, S.B., Hersbach, H., Hólm, E.V., Isaksen, L., Kållberg, P., Köhler, M., Matricardi, M., McNally, A.P., Monge-Sanz, B.M., Morcrette, J.-J., Park, B.-K., Peubey, C., de Rosnay, P., Tavolato, C., Thépaut, J.-N., and Vitart, F.: The ERA-Interim reanalysis: Configuration and
545 performance of the data assimilation system, *Q. J. R. Meteorol. Soc.*, 137, 553–597, <https://doi.org/10.1002/qj.828>, 2011.
- Essou, G.R.C., Arsenault, R., and Brissette, F.P.: Comparison of climate datasets for lumped hydrological modeling over the continental United States, *J. Hydrol.*, 537, 334–345, <https://doi.org/10.1016/j.jhydrol.2016.03.063>, 2016.
- Fountain, A.G., Campbell, J.L., Schuur, E.A.G., Stammerjohn, S.E., Williams, M.W., and Ducklow, H.W.: The
550 disappearing cryosphere: Impacts and ecosystem responses to rapid cryosphere loss, *BioScience*, 62(4), 405–415, <https://doi.org/10.1525/bio.2012.62.4.11>, 2012.
- Frogner, I.-L., Singleton, A.T., Køltzow, M.Ø., and Andrae, U.: Convection-permitting ensembles: Challenges related to their design and use, *Q. J. R. Meteorol. Soc.*, 145(Suppl. 1), 90–106, <https://doi.org/10.1002/qj.3525>, 2019.
- 555 Førland, E.J., Hanssen-Bauer, I., Jónsson, T., Kern-Hansen, C., Nordli, P.Ø., Tveito, O.E., and Laursen, E.V.: Twentieth-century variations in temperature and precipitation in the Nordic Arctic, *Polar Rec.*, 38(206), 203–210, <https://doi.org/10.1017/S0032247400017721>, 2002.
- Gandin, L.S.: Objective analysis of meteorological fields, Translated from Russian, Jerusalem (Israel Program for Scientific Translations), 242 pp., <https://doi.org/10.1002/qj.49709239320>, 1965.
- 560 Grusson, Y., Wesström, I., and Abraham, J.: Impact of climate change on Swedish agriculture: Growing season rain deficit and irrigation need, *Agric. Water Manag.*, 251, 106858, <https://doi.org/10.1016/j.agwat.2021.106858>, 2021.



- Harris, I., Jones, P.D., Osborn, T.J., and Lister, D.H.: Updated high-resolution grids of monthly climatic observations – the CRU TS4.05 dataset, *Int. J. Climatol.*, 40(11), 5280–5292, 565 <https://doi.org/10.1002/joc.3711>, 2020.
- Hersbach, H., Bell, B., Berrisford, P., Hiahara, S., Horányi, A., Muñoz-Sabater, J., Nicolas, J., Peubey, C., Radu, R., Schepers, D., Simmons, A., Soci, C., AbdALLA, s., Abellan, X., Balsamo, G., Bechtold, P., Biavati, G., Bidlot, J., Bonavita, M., De Chiara, G., Dahlgren, P., Dee, D., Diamantakis, M., Dragani, R., Flemming, J., Forbes, R., Fuentes, M., Geer, A., Haimberger, L., Healy, S., Hogan, R. J., Hólm, E., Janisková, M., Keeley, S., Laloyaux, P., 570 Lopez, P., Lupu, C., Radnoti, G., de Rosnay, P., Rozum, I., Vamborg, F., Villaume, S., and Thépaut, J-N.: The ERA5 global reanalysis, *Q. J. R. Meteorol. Soc.*, 146, 1999–2049, <https://doi.org/10.1002/qj.3803>, 2020.
- Haylock, M.R., Hofstra, N., Klein Tank, A.M.G., Klok, E.J., Jones, P.D., and New, M.: A European daily high-resolution gridded data set of surface temperature and precipitation for 1950–2006, *J. Geophys. Res. Atmos.*, 113, D20119, <https://doi.org/10.1029/2008JD010201>, 2008.
- 575 IPCC: Sixth assessment report (AR6): The physical science basis, Intergovernmental Panel on Climate Change, <https://www.ipcc.ch/report/ar6/wg1/>, 2021.
- IPCC: Summary for policymakers, in *Climate Change 2013: The Physical Science Basis. Contribution of Working Group I to the Fifth Assessment Report of the Intergovernmental Panel on Climate Change*, edited by Stocker, T.F. et al., Cambridge Univ. Press, Cambridge, U.K., and New York, pp. 3–29, 2013.
- 580 Klein Tank, A. M. G., Wijngaard, J. B., Können, G.P., Böhm, R., Demarée, G., Gocheva, A., Mileta, M., Pashiardis, S., Hejkrlik, L., Kern-Hansen, C., Heino, R., Bessemoulin, P., Müller-Westermeier, G., Tzanakou, M., Szalai, S., Pálsdóttir, T., Fitzgerald, D., Rubin, S., Capaldo, M., Maugeri, M., Leitlase, A., Bukantis, A., Aberfeld, R., van Engelen, A. F. V., Forland, E., Miletus, M., Coelho, F., Mares, C., Razuvaev, V., Nieplova, E., Cegnar, T., Antonio López, J., Dahlström, B., Moberg, A., Kirchhofer, W., Ceylan, A., Pachaliuk, O., Alexander, L. V., and Petrovic, 585 P.: Daily dataset of 20th-century surface air temperature and precipitation series for the European Climate Assessment, *Int. J. Climatol.*, 22(12), 1441–1453, <https://doi.org/10.1002/joc.773>, 2002.
- Klok, E.J. and Klein Tank, A.M.G.: Updated and extended European dataset of daily climate observations, *Int. J. Climatol.*, 29(8), 1182–1191, <https://doi.org/10.1002/joc.1779>, 2009.



- Lind, P., Belušić, D., Médus, E., Dobler, A., Pedersen, R.A., Wang, F., Matte, D., Kjellström, E., Landgren, O.,
590 Lindstedt, D., Christensen, O.B., and Christensen, J.H.: Climate change information over Fenno-Scandinavia
produced with a convection-permitting climate model, *Clim. Dyn.*, 61, 519–541, <https://doi.org/10.1007/s00382-022-06589-3>, 2023.
- Le Moigne, P., Besson, F., Martin, E., Boé, J., Boone, A., Decharme, B., Etchevers, P., Faroux, S., Habets, F.,
Lafaysse, M., Leroux, D., and Rousset-Regimbeau, F.: The latest improvements with SURFEX v8.0 of the
595 Safran–Isba–Modcou hydrometeorological model for France, *Geosci. Model Dev.*, 13, 3925–3946,
<https://doi.org/10.5194/gmd-13-3925-2020>, 2020.
- Lussana, C., Uboldi, F., and Salvati, M.R.: A spatial consistency test for surface observations from mesoscale
meteorological networks. *Quarterly Journal of the Royal Meteorological Society*, 136(649), 1075–1088,
<https://doi.org/10.1002/qj.622>, 2010.
- 600 Lussana, C., Saloranta, T., Skaugen, T., Magnusson, J., Tveito, O.E., and Andersen, J.: seNorge2 daily
precipitation, an observational gridded dataset over Norway from 1957 to the present day, *Earth Syst. Sci. Data*,
10, 235–249, <https://doi.org/10.5194/essd-10-235-2018>, 2018.
- Lussana, C., Tveito, O.E., Dobler, A., and Tunheim, K.: seNorge_2018, daily precipitation and temperature datasets
over Norway, *Earth Syst. Sci. Data*, 11, 1331–1351, <https://doi.org/10.5194/essd-11-1531-2019>, 2019.
- 605 Mankin, K.R., Mehan, S., Green, T.R., and Barnard, D.M.: Review of Gridded Climate Products and Their Use in
Hydrological Analyses Reveals Overlaps, Gaps, and Need for More Objective Approach to Model Forcings,
Hydrol. Earth Syst. Sci. Discuss. [preprint], <https://doi.org/10.5194/hess-2024-58>, in review, 2024.
- Monteiro, D. and Morin, S.: Multi-decadal analysis of past winter temperature, precipitation and snow cover data
in the European Alps from reanalyses, climate models and observational datasets, *The Cryosphere*, 17, 3617–3660,
610 <https://doi.org/10.5194/tc-17-3617-2023>, 2023.
- Mikkonen, S., Laine, M., Mäkelä, H., Gregow, H., Tuomenvirta, H., Lahtinen, M., and Laaksonen, A.: Trends in
the average temperature in Finland, 1847–2013, *Stoch. Environ. Res. Risk Assess.*, 29(6), 1521–1529,
<https://doi.org/10.1007/s00477-014-0992-2>, 2015.



615 Nikulin, G., Kjellström, E., Hansson, U., et al.: Evaluation and future projections of temperature, precipitation and
wind extremes over Europe in an ensemble of regional climate simulations, *Tellus A Dyn. Meteorol. Oceanogr.*,
63(1), 41, <https://doi.org/10.1111/j.1600-0870.2010.00466.x>, 2011.

Overpeck, J.T., Meehl, G.A., Bony, S., and Easterling, D.R.: Climate data challenges in the 21st century, *Science*,
331(6018), 700–702, <https://doi.org/10.1126/science.1197869>, 2011.

620 Raza, A., Partonen, T., Magnusson Hansson, L., Asp, M., Engström, E., Westerlund, H., and Halonen, J.I.: Daylight
during winter and symptoms of depression and sleep problems: A within-individual analysis, *Environ. Int.*, 183,
108413, <https://doi.org/10.1016/j.envint.2023.108413>, 2024.

Schimanke, S., Ridal, M., Le Moigne, P., Berggren, L., Undén, P., Randriamampianina, R., Andrea, U., Bazile, E.,
Bertelsen, A., Brousseau, P., Dahlgren, P., Edvinsson, L., El Said, A., Glinton, M., Hopsch, S., Isaksson, L.,
625 Mladek, R., Olsson, E., Verrelle, A., and Wang, Z.Q.: CERRA sub-daily regional reanalysis data for Europe on
single levels from 1984 to present, Copernicus Climate Change Service (C3S) Climate Data Store (CDS),
<https://doi.org/10.24381/cds.622a565a>, 2021.

Soci, C., Bazile, E., Besson, F., and Landelius, T.: High-resolution precipitation re-analysis system for
climatological purposes, *Tellus A*, 68, <https://doi.org/10.3402/tellusa.v68.29879>, 2016.

SOU: Sweden facing climate change—threats and opportunities, Swedish Government Official Reports, Report
630 2007:60, <https://www.government.se/legal-documents/2007/12/sou-200760/>, 2007.

Themeßl, M.J., Gobiet, A., and Heinrich, G.: Empirical-statistical downscaling and error correction of regional
climate models and its impact on the climate change signal, *Climatic Change*, 112, 449–468,
<https://doi.org/10.1007/s10584-011-0224-4>, 2012.

635 Tietäväinen, H., Tuomenvirta, H., and Venäläinen, A.: Annual and seasonal mean temperatures in Finland during
the last 160 years based on gridded temperature data, *Int. J. Climatol.*, 30(15), 2247–2256,
<https://doi.org/10.1002/joc.2046>, 2010.

Tveito, O.E. and Lussana, C.: The Nordic Gridded Climate Dataset stable release, ECMWF Copernicus note,
Copernicus Climate Change Service, 29 pp.,



640 https://surfobs.climate.copernicus.eu/documents/C3S_M311a_Lot4.2.3.3_201809_report_stable_release_v1.pdf,
last access: 30 September 2025, 2018.

Yu, Y., Schneider, U., Yang, S., Becker, A., and Ren, Z.: Evaluating the GPCP Full Data Daily Analysis Version 2018 through ETCCDI indices and comparison with station observations over mainland of China, *Theor. Appl. Climatol.*, 142, 835–845, <https://doi.org/10.1007/s00704-020-03352-8>, 2020.

645 Zandler, H., Haag, I., and Samimi, C.: Evaluation needs and temporal performance differences of gridded precipitation products in peripheral mountain regions, *Sci. Rep.*, 9, 15118, <https://doi.org/10.1038/s41598-019-51666-z>, 2019.